IEEE Photonics Journal
An IEEE Photonics Society Publication

Open Access

Characterization of a Downconverting, Phase-Modulated RF-Over-Fiber Link With a Single Modulator

Volume 10, Number 4, August 2018

Bryan M. Haas, *Member, IEEE*
Jason D. McKinney, *Senior Member, IEEE*

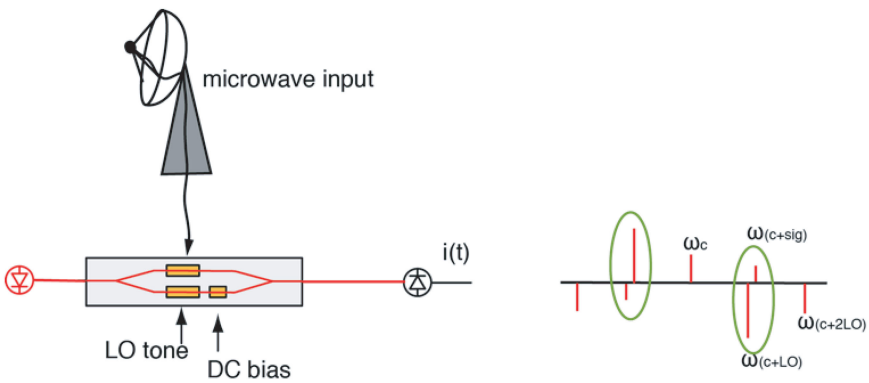

(a) (b)

DOI: 10.1109/JPHOT.2018.2846415
1943-0655 © 2018 U.S. Government

IEEE photonics SOCIETY

IEEE

Characterization of a Downconverting, Phase-Modulated RF-Over-Fiber Link With a Single Modulator

Bryan M. Haas, ***Member, IEEE***,
and Jason D. McKinney, ***Senior Member, IEEE***

United States Naval Research Laboratory, Washington, DC 20375 USA

DOI:10.1109/JPHOT.2018.2846415

Manuscript received May 22, 2018; revised June 6, 2018; accepted June 7, 2018. Date of publication June 11, 2018; date of current version July 4, 2018. Corresponding author: Bryan M. Haas (e-mail: bryan.haas@nrl.navy.mil).

Abstract: We present and fully characterize a downconverting RF-over-fiber link that uses one dual-RF drive Mach–Zehnder modulator as a phase modulator. One RF input presents the signal and the other input presents the local oscillator to the modulator. A full link characterization and experimental comparison with the developed theory is presented for the first time, verifying the relevant RF metrics that can be immediately useful in a practical system design.

Index Terms: Dual-drive Mach-Zehnder modulator, frequency downconversion, microwave photonics, microwave mixers, carrier suppression, radio over fiber.

1. Introduction

Wide-Bandwidth digitizers have revolutionized radio engineering over the past decade. The ability to digitize and demodulate multiple waveforms within a bandwidth of several hundred MHz to around 1 GHz has vastly reduced the physical complexity of large systems, eliminating banks of narrow-band amplifiers, filters, mixers, and receivers. However, technology has not yet progressed to allow direct demodulation of complex signals (e.g., 256QAM) when the carrier frequency is above approximately L-band. Therefore, when the signal(s) of interest are higher than this, some downconversion to a useable IF is still necessary. A variety of microwave photonic techniques [1]–[4] have been developed to enable this and eliminate electronic mixers while also allowing signal relay.

The link described in this letter and shown in Fig. 1 is the same as [5], which, to our knowledge, was the first demonstration of a DDMZM re-purposed as a parallel phase modulator in a microwave photonics context (DDMZMs are typically used for digital DPSK modulation or as a low-$V\pi$ intensity modulator). This design can be viewed as a version of [6], [7] which re-purposed a commercial QPSK MZM (i.e., 2 separate MZMs nested within a parent MZM, with each of the 3 MZMs biased separately) to downconvert signals. These links, as well as a version optimized for phase shifting [8], are elegant in that, depending on the modulator phase bias(es), they can either act as phase modulators that efficiently downconvert a signal to IF, or as intensity modulators that relay the signal at the original RF. None of the realizations have a lower limit on the RF frequency that can be downconverted, an advantage over some other designs [9] that, in principle, allows the same link to be used regardless of the input frequency, within the upper limits of the modulator and detector.

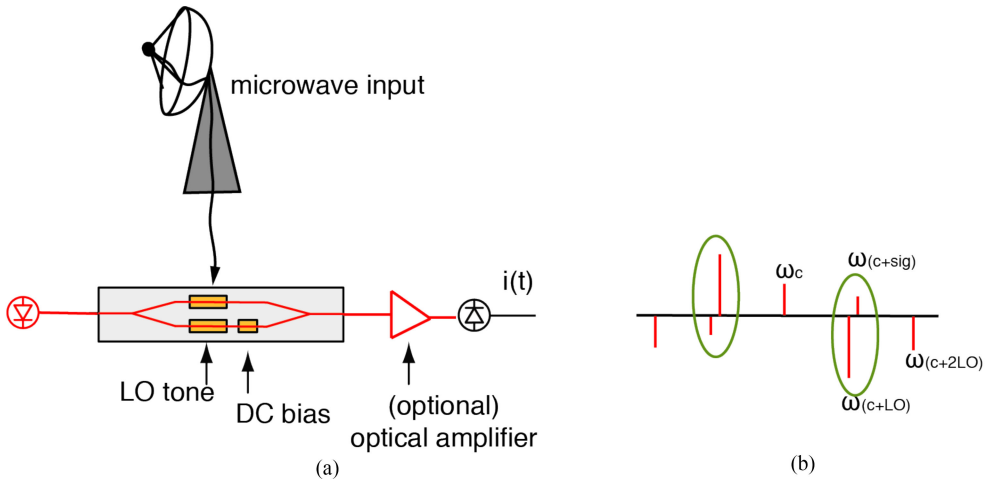

Fig. 1. (a) Schematic of the downconverting DDMZM link. (b) Representative spectrum at the modulator output; IF beats that combine in the detector are circled. Pi phase bias in the lower arm causes the carrier and LO sidebands to be antiphased from the signal, which partially suppresses the carrier and allows the IF to be directly detected.

The previous [5] work focused on proof-of-concept and verified that a complex 16QAM K_a-band signal could be downconverted, with minimal degradation, in a single step to L-band. Although [5] experimentally verified that the design works, the underlying theoretical performance was not developed. Therefore, it is not known whether the design as previously described performs as expected and it cannot be quantitatively compared with other link designs. This paper presents a full link characterization that will be useful to one who seeks to compare this design to other candidate designs or include it in a system cascade analysis. Given the multitude of other downconverting link designs, we do not seek in this paper to explicitly compare this design with others. In particular, expressions for the gain (G), noise figure (NF), and spur-free dynamic range (SFDR) are developed for the shot-noise and amplifier noise-limited cases, and experimentally verified.

2. Theory

A continuous-wave optical carrier is incident upon the DDMZM. Within the modulator, one arm is phase modulated with the RF signal(s) of interest (here a single-frequency tone for simplicity) and the other arm is modulated with the LO frequency. The modulator's output optical spectrum is shown in Fig. 1 and represented as

$$E(t) = \sqrt{P_0} e^{j\omega_c t} \left[\sum_{n=-\infty}^{\infty} J_n(m_s)\, e^{jn\Omega_s t} + e^{j\varphi} \sum_{p=-\infty}^{\infty} J_n(m_{LO})\, e^{jp\Omega_{LO} t} \right] \tag{1}$$

where P_0 is the optical carrier power input to the modulator, m_s is the signal modulation depth defined as $m_s = (\pi V_0)/V_\pi$ (V_π is the single-drive halfwave voltage of the modulator), ω_c is the optical carrier frequency, Ω_s is the microwave signal frequency, φ is the static optical phase difference between the two arms of the MZM, m_{LO} is the LO modulation depth and Ω_{LO} is the LO frequency.

This field propagates through the fiber link and is incident upon a photodiode, with the resultant electrical output:

$$i(t) = \frac{\Re P_0 \alpha}{4} \left[\begin{array}{c} J_0^2(m_{LO}) + J_0^2(m_s) + 2J_1^2(m_{LO}) + 2J_1^2(m_s) + 2J_0(m_{LO}) J_0(m_s) \cos(\varphi) \\ + 2J_1(m_{LO}) J_1(m_s) (\cos(\Omega_{IF} + \varphi) + \cos(\Omega_{IF} - \varphi)) \end{array} \right] \tag{2}$$

Only the carrier and first sidebands have been retained, for clarity. $\Re$ is the photodiode responsivity, α is attenuation through the link (optical loss between the modulator input and detector) and

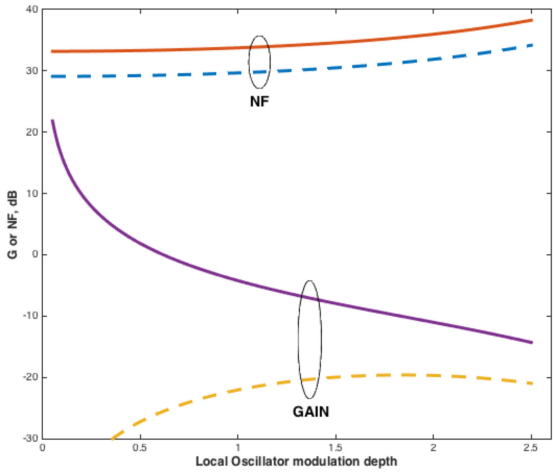

Fig. 2. Plot of conversion gain and link NF vs LO modulation depth for constant input power/shot-noise limited (dashed) and constant output DC current/EDFA-noise limited (solid) cases, with the EDFA placed after the modulator. Input optical power is 17 dBm, link loss is 5 dB, EDFA optical NF is 6 dB, detector responsivity is 0.8 A/W, and photocurrent for the constant DC current case is 10mA.

Ω_{IF} is the IF, defined as the beat frequency ($\Omega_{LO} - \Omega_s$). If the static phase is set to π, the outputs from the 2 arms are exactly antiphased. This is commonly known as "biasing at null" or carrier-suppressed biasing. Under this condition, and with small signal modulation depth ($m_s << 1$), (2) simplifies to:

$$i(t) = \frac{\Re P_0 \alpha}{4}\left[1 + J_0^2(m_{LO}) - 2J_0(m_{LO}) + 2J_1^2(m_{LO}) - 2J_1(m_{LO})\, m_s \cos(\Omega_{IF} t)\right]. \quad (3)$$

Despite being "carrier suppressed" at null bias, there is some carrier contribution in the DC component of the output, evidenced by the J_0 terms. The incompletely suppressed carrier is caused by unequal modulation depths in each arm of the DDMZM. A typically large LO modulation depth desensitizes the carrier in that arm of the MZM and cannot perfectly cancel the large carrier amplitude in the lightly-modulated signal arm. When used as an intensity or DPSK modulator, each arm of a DDMZM is modulated to the same depth, which can result in full carrier suppression. This can still occur here if the LO and signal modulation depths in (2) are the same, even at different RF frequencies. A full analysis must include the higher-order sidebands, which for large modulation depths can contribute measureable optical power and therefore DC photocurrent. Alternately, one can optically filter these higher-frequency components prior to detection.

The IF is efficiently recovered because the signal is beating against an LO which is significantly smaller than the original carrier [J_1(m) maximizes at 0.58 of the carrier amplitude] thus making the apparent modulation depth at the detector larger. This compensates for the reduced optical power at the detector, while that reduced optical power also generates less shot noise and can therefore decrease the noise figure.

2.1 RF Link Metrics

Knowing the output electrical current, we may now determine the relevant link metrics to facilitate comparison with other techniques or components, and with which to enable a system cascade analysis. The primary metrics to develop and verify are RF gain (conversion efficiency) and RF noise figure, plotted in Fig. 2. From these, spur-free dynamic range is derived.

RF gain is the ratio of output RF power (in this case at the IF) to input RF signal power. Under the conditions that led to (3) and designating the time-dependent component of (3) as i_{sig}:

$$G_{RF} = \frac{\langle i_{sig}^2 \rangle z_{out}}{\left(v_{rms}^2 / z_{in}\right)} = (\Re P_0 \alpha)^2 \left[J_1^2 (m_{LO}) \left(\frac{\pi^2 R_{in} R_{out}}{4 V_\pi^2} \right) \right] \tag{4}$$

which is the same result as the intensity-modulated link from [6] when one takes α here to subsume both the amplifier gain and modulator loss terms in [6]; the apparent difference of ¼ from their result is due to the factor of 2 between V_π of the single- and dual-drive configurations, also described in [6]. R_{in} and R_{out} are the generator and load resistances seen by the modulator and detector, respectively.

So long as all significant components in the received current can be accounted for (i.e., LO harmonics), it is often convenient to express G in terms of the DC photocurrent. This is an easily accessible measurement that enables quick performance verification in a lab or field environment. For the 1st-order case presented here,

$$G_{RF} = {i_{DC}}^2 \left[\left(\frac{J_1 (m_{LO})}{\left(1 + J_0^2 (m_{LO}) - 2J_0 (m_{LO}) + 2J_1^2 (m_{LO})\right)} \right)^2 \left(\frac{4\pi^2 R_{in} R_{out}}{V_\pi^2} \right) \right]. \tag{5}$$

A link with fixed attenuation (e.g., unamplified) is most easily represented by a fixed input optical power as in (4). Received optical power will vary with the LO modulation depth, and gain is maximized when $J_1(m_{LO})$ is largest; this occurs when $m_{LO} \sim 1.83$.

Alternatively, for a link with variable attenuation or amplification that enables a constant received optical power, (5) can be more instructive. In this case gain increases as LO modulation depth decreases, as was asserted and verified in [6]. This increase is limited in practice as m_{LO} approaches m_{sig}; the effective modulation depth, or relative amplitudes of the signal and LO as they beat, becomes large and the assumptions made in (3) are no longer valid.

Noise figure is the ratio of input to output signal-to-noise ratios:

$$NF = \frac{SNR_{in}}{SNR_{out}} = \frac{S_o}{G_{RF} kT}. \tag{6}$$

S_o is the output noise power spectral density (PSD), k is Boltzman's constant, and T is absolute temperature, taken to be 290 degrees Kelvin. For the shot-noise limited case, $S_o = 2q < i_{DC} > R_0$ where q is the fundamental electronic charge. NF in terms of input power and output DC current, respectively, is:

$$\begin{aligned} NF_{shot} &= \frac{1}{(\Re P_0 \alpha)} \left[\frac{2q \left(1 + J_0^2 (m_{LO}) - 2J_0 (m_{LO}) + 2J_1^2 (m_{LO})\right) V_\pi^2}{J_1^2 (m_{LO}) \pi^2 R_{in} kT} \right] \\ &= \frac{1}{i_{DC}} \left[\frac{q\left(1 + J_0^2 (m_{LO}) - 2J_0 (m_{LO}) + 2J_1^2 (m_{LO})\right)^2 V_\pi^2}{2J_1^2 (m_{LO}) \pi^2 R_{in} kT} \right]. \end{aligned} \tag{7}$$

For a fixed m_{LO}, NF_{shot} is inversely proportional to optical power (or DC current). Gain increases quadratically with current while shot noise power increases linearly; doubling the DC current results in a net doubling of the output SNR. If m_{LO} is allowed to vary, NF_{shot} rises monotonically with m_{LO} and fixed input power.

If an optical amplifier, specifically an Erbium-doped fiber amplifier (EDFA), is present, the signal-spontaneous (s-sp) noise generally dominates when the amplifier gain is $>>1$. In this case [10],

$$S_o = \langle i_{DC}^2 \rangle z_{out} \left(\frac{2h\upsilon NF_{EDFA}}{P_{opt,\ in}} \right) \tag{8}$$

where h is Planck's constant, v is the optical frequency, NF_{EDFA} is the optical noise figure of the EDFA, and $P_{opt,\,in}$ is the optical power input to the EDFA (not the same as P_0). The RF noise figure

then becomes:

$$NF_{\text{ssp}} = \frac{\left(1 + J_0^2\left(m_{LO}\right) - 2J_0\left(m_{LO}\right) + 2J_1^2\left(m_{LO}\right)\right)^2 V_\pi^2}{4J_1^2\left(m_{LO}\right)\pi^2 R_{\text{in}} kT}\left(\frac{2h\upsilon NF_{\text{EDFA}}}{P_{\text{opt,in}}}\right). \tag{9}$$

As expected, there is no explicit dependence upon received optical power or DC current, as RF gain and s-sp noise have the same dependence and cancel. There is a dependence on the optical power input to the EDFA, which will vary with m_{LO} if placed after the modulator.

Spur-free dynamic range is calculated in the usual way using NF, where the input-referenced 3rd-order intercept point (IIP3) from [11] is $4V_\pi^2/\pi^2 z_{\text{in}}$. The full expressions for this link are somewhat unwieldy and do not yield particularly novel insight so the general expression is provided, with SFDR calculable from the metrics given above:

$$SFDR\left(Hz^{2/3}\right) = \left(\frac{IIP3}{NFkT}\right)^{2/3} \tag{10}$$

3. Experimental Verification and Discussion

Measurements were made to verify the primary metrics: gain and NF, from (4), (5), (7), and (9). A DDMZM with 4.5 dB optical insertion loss at "full on" bias and 5.6 V measured single-drive V_π at 20 GHz in each arm was illuminated by a 50 mW fiber laser at 1550 nm, verified as shot-noise limited above 2 MHz. A 19.5 GHz signal drive was set to a low power, −20 dBm, and a 20 GHz LO was set to deliver 18.3 dBm to the modulator, the maximum drive that could be supplied by the generator. This resulted in $m_{LO} \sim 1.47$. The detector was a 10 GHz-bandwidth photodiode with 0.8 A/W responsivity, internal 50-Ohm parallel matching resistor, and linear power handling up to at least 20 mA. Connectors accounted for an additional 0.5 dB of optical loss, resulting in 16 mW CW power arriving at the photodiode when the modulator was biased to "full on" and no LO or signal was applied. When the LO and signal were applied and the modulator was biased at null, the DC photocurrent was 3 mA and the measured 500 MHz IF was −46.5 dBm. This measured −26.5 dB G_{RF} compares favorably with the −26 dB calculated link gain from both (4) and (5), after subtracting 6 dB from the calculated results due to the matching resistor in the photodiode that acts as a current divider [12].

The measured noise PSD was −165 dBm/Hz, within 0.5 dB of the calculated value when taking shot and thermal noise into account (the system is not quite shot-limited with only 3 mA of photocurrent). Subtracting the thermal noise contribution, the shot noise PSD was −165.7 dBm/Hz. From (6) and using the measured gain from above, the measured NF was 34.8 dB whereas the calculated NF directly from (7) was 33.9 dB, exactly in line with the measured value when accounting for the 1/2 dB difference between measured and calculated values for both gain and PSD. Again, care must be taken to account for matching resistors; dividing the current by 2 increases the NF from (7) by 3 dB. Demonstrating the importance of accounting for other spectral components, (5) was adapted in all of the above calculations to account for the unfiltered 2nd harmonic of the LO, which was large enough to add to the DC photocurrent. Without this correction, the calculated gain from (5) exactly as written would have been 25 dB.

To verify the amplifier-limited NF (9), the modulator output was attenuated to −9 dBm and an EDFA with a 6 dB optical NF was placed before the detector. The input power to the EDFA was reduced to ensure it was operating in the small-signal amplification regime such that (8) and (9) would hold. The measured 11 mA photocurrent and measured −14.5 dB RF gain matched the predicted value (−8.5 dB) before accounting for the resistor. Likewise, the −138.5 dBm/Hz measured PSD compares with the calculated −139 dBm/Hz PSD. Using the measured values with (6) gives a 50 dB NF, matching that calculated from (9).

SFDR and NF were measured in the shot-noise limited case with a two-tone test using tones at 19.5 and 19.51 GHz with the 20 GHz LO again set to a 1.47 modulation depth. The power incident upon the modulator was increased for this part of the experiment, resulting in a net 8.8 mA of DC photocurrent when biased to null and with the LO on. The downconverted 3rd-order intermodulation

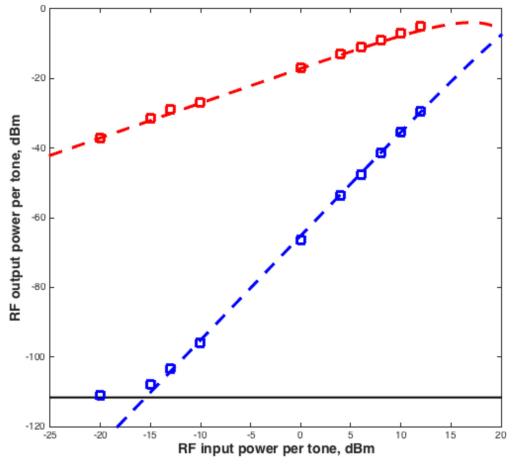

Fig. 3. Plot of measured and calculated powers showing good agreement between fundamental (red), 3rd-order IMD (blue) and noise (black) components for the shot-noise limited case with 100 kHz Resolution Bandwidth.

products (IMD) at 480 and 510 MHz were measured and plotted along with the IF tone powers and measured noise floor, shown in Fig. 3. The measured data is in good agreement with the calculated powers and noise with −17 dB gain, a 29.5 dB noise figure, and 112 dBHz$^{2/3}$ shot-noise limited SFDR.

The experimental results show that this is an average-performance link with the on-hand components. With state-of-the-art devices, Gain and Noise Figure can be improved in the usual ways by combinations of decreasing modulator V_π and increasing the non-amplified received optical power (and detector power handling). Even then, the primary benefit of this design is simplicity. As an example, using a state-of-the-art modulator with a 2 V single-drive V_π and 2 dB optical insertion loss in the experiment of the previous paragraph would improve the Gain by ∼14 dB (9 dB from the lower V_π and 5 dB from the increased photocurrent) to −3 dB and improve the Noise Figure by ∼11.5 dB (9 dB from the lower V_π and 2.5 dB from the increased photocurrent) to 18 dB. At this value, only a very modest electronic low-noise pre-amplifier (LNA) might be necessary, if at all, depending upon the use case. The link's SFDR would only improve by 1.6 dB, as both IP3 and NF have the same dependence upon V_π, thus only the NF improvement due to the higher received optical power improves SFDR.

4. Conclusion

We have extended previous efforts and developed a link characterization that will be useful to one who seeks to compare this design to other candidate designs or include it in a system cascade analysis. RF gain and noise figure were derived and experimentally verified in terms of both input power and output current to facilitate quick calculations with whichever means the user finds more convenient. By showing different formulations, we have pointed out some of the various operating points to optimize G, NF, and/or SFDR in both the shot- and amplifier-limited noise regimes. This newly developed theory can guide an interested party to various adaptations that would suit their particular application space.

References

[1] G. K. Gopalakrishnan, W. K. Burns and C. H. Bulmer, "Microwave-optical mixing in LiNbO3 modulators," *IEEE Trans. Microw. Theory Techn.*, vol. 41, no. 12, pp. 2383–2391, Dec. 1993.

[2] V. R. Pagán, B. M. Haas, and T. E. Murphy, "Linearized electrooptic microwave downconversion using phase modulation and optical filtering," *Opt. Exp.*, vol. 19, pp. 883–895, 2011.

[3] T. R. Clark and M. L. Dennis, "Linear microwave downconverting RF-to-bits link," in *Proc. 2008 Int. Top. Meeting Microw. Photon., Asia-Pacif. Microw. Photon. Conf.*, Gold Coast, QLD, Canada, 2008, pp. 12–14.
[4] R. Helkey, J. C. Twichell and C. Cox, "A down-conversion optical link with RF gain," *J. Lightw. Technol.*, vol. 15, no. 6, pp. 956–961, Jun 1997.
[5] Z. Tang, F. Zhang, D. Zhu, X. Zou and S. Pan, "A photonic frequency downconverter based on a single dual-drive Mach-Zehnder modulator," in *Proc. 2013 IEEE Int. Top. Meeting Microw. Photon.*, Alexandria, VA, USA, 2013, pp. 150–153.
[6] E. H. W. Chan and R. A. Minasian, "Microwave photonic downconverter with high conversion efficiency," *J. Lightw. Technol.*, vol. 30, no. 23, pp. 3580–3585, Dec.1, 2012.
[7] Y. Wang *et al.*, "All-optical microwave photonic downconverter with tunable phase shift," *IEEE Photon. J.*, vol. 9, no. 6, Dec. 2017, Art. no. 5503408.
[8] T. Jiang, S. Yu, R. Wu, D. Wang, and W. Gu, "Photonic downconversion with tunable wideband phase shift," *Opt. Lett.*, vol. 41, pp. 2640–2643, 2016.
[9] B. M. Haas and T. E. Murphy, "A carrier-suppressed phase-modulated fiber optic link with IF downconversion of 30 GHz 64-QAM signals," in *Proc. 2009 Int. Top. Meeting Microw. Photon.*, 2009, pp. 1–4.
[10] E. Desurvire, *Erbium Doped Fiber Amplifiers: Principles and Applications*, New York, NY, USA: Wiley, 1994.
[11] B. H. Kolner and D. W. Dolfi, "Intermodulation distortion and compression in an integrated electrooptic modulator," *Appl. Opt.*, vol. 26, pp. 3676–3680, 1987.
[12] V. Urick, K. Williams, and J. McKinney, *Fundamentals of Microwave Photonics*, New York, NY, USA: Wiley, 2015.